Applications of the 3-D Navier-Stokes Code OVERFLOW for Analyzing Propulsion-Airframe Integration Related Issues on Subsonic Transports

L. M. Gea[*], N. D. Halsey[**], G. A. Intemann[***]
Transonic Aerodynamics Technology
McDonnell Douglas Aerospace - West
Long Beach, California

P. G. Buning[§]
NASA Ames Research Center
Moffett Field, California

Abstract

The three-dimensional thin-layer Navier-Stokes computational fluid dynamics (CFD) code OVERFLOW with Chimera overset grid approach has been applied to the detailed analysis of a complete subsonic transport aircraft wing/fuselage/nacelle/pylon configuration. A grid procedure to treat the complicated engine installation geometry is presented in this paper, including a detailed discussion of the grid generation for the individual geometry components and the PEGSUS process for finding the appropriate interpolations between the overset grids. A key objective of the analyses was to validate/calibrate OVERFLOW for analyzing propulsion-airframe installation effects. Numerical issues such as turbulence models, differencing schemes, and convergence rate are discussed to assess the code performance. The calculated results for wing/fuselage and wing/fuselage/nacelle/pylon configurations are compared to the available wind-tunnel test data. Good correlation between the test data and the predicted results demonstrates the capability of the OVERFLOW code for propulsion-airframe integration analyses.

I. Introduction

A critical aspect of advanced subsonic transport aircraft design is the minimization of adverse interference in junction regions between major components of the vehicle, such as in the wing/pylon and nacelle/pylon junctions. This statement is underscored by recent trends in subsonic aircraft design which have resulted in the requirement for efficient wing-integration of increasingly larger, higher bypass-ratio (BPR) nacelles. The vehicle performance gains targeted with these higher BPR engines could easily be negated by potential adverse interference effects arising from inefficient installation designs. The required design processes for efficient wing engine integration rely heavily on calibrated full-configuration CFD methodologies. Development of these calibrated full-configuration CFD design and analysis processes will greatly benefit future and existing subsonic transport aircraft development.

Currently, CFD algorithms and computer architecture have progressed to the stage that Navier-Stokes and Euler analyses for complicated full-configuration geometries are possible. However, a primary obstacle to these analyses arise due to the difficulty of generating an appropriate grid system. Two different types of grid systems have been widely used. The first are unstructured grids[1,2], which have the flexibility of handling complex geometries and the capability of obtaining solution grid adaptation, making them a very attractive approach. However, viscous implementation for complex 3-D geometries is still in need of further improvement. The second grid system widely used are structured grids[3,4,5], which have the advantage of more compatibility with the viscous grid requirements of Navier-Stokes flow solvers. Unfortunately, generating structured grids around complicated full-configuration geometries poses a challenge.

A zonal approach is commonly employed for structured grids, whereby the entire computational domain is broken into several subdomains. Careful selection of the zone topology can simplify the grid generation about individual components of the configuration and also allow for more accurate calculation of the

---

flow physics in specific areas. Depending on the treatment at the zone boundaries, three different categories of structured grid systems can be defined: point-matched[6], surface-patched[7], and overset[8] grids. Different interpolation algorithms are imposed at the zone boundaries to ensure the necessary computational communication between adjoining grid zones. The advantage of maintaining flux conservation at the zonal boundaries by using surface-patched and point-matched grids is offset by the often tedious grid generation process, especially when a viscous layer is involved. In contrast, overset grids have almost no constraints at zone boundaries other than requiring overlapped regions between the adjacent zones. This not only reduces the effort in generating grids, but also provides great flexibility in modifying individual zone grids for further design purposes.

The Chimera overset grid approach was originally developed for wing-store separation calculations. Later it was expanded for treating various complex geometry problems, as for instance a multiple-body space shuttle full-configuration[9], or a 2-D high-lift multi-element configuration[10]. For both cases, the grid generation for these extremely complex geometries in conjunction with the viscous mesh requirements were handled successfully with overset grids. Furthermore, the results correlate well with wind-tunnel test data and lend credence to the application of this overset procedure to the current propulsion-airframe integration analyses. This paper focuses on the discussion of using overlapping grids for complex propulsion-airframe integration analyses.

OVERFLOW[11], a NASA Ames developed thin-layer Navier-Stokes code with Chimera overset grid approach[12,13], was chosen for the analyses. A commercial twinjet transport aircraft with advanced transonic wing, which was extensively tested at NASA Langley Research Center is studied. The engine geometry modeled includes a nacelle, pylon, core-cowl, and core-cowl bifurcation, as seen in Fig. 1. This engine configuration is seen to be a flow through wind-tunnel test geometry. The approach used to calibrate OVERFLOW first compared the calculated results to National Transonic Facility (NTF) wind-tunnel test data for the wing/fuselage only. In this manner, several numerical issues such as turbulence model, discretization algorithm, and code convergence

properties are studied to establish the general characteristics and application guidelines for using OVERFLOW. Next, OVERFLOW results for the complete wing/fuselage/nacelle/pylon configuration were obtained and correlated with corresponding NTF wind-tunnel test data.

Section II discusses the overset grid generation details for the different vehicle components. The OVERFLOW governing equations and numerical procedures are briefly described in Section III. A discussion of computational results and conclusions are found in Sections IV and V, respectively.

II. Grid Generation

The Chimera approach greatly simplifies the task of generating a grid about a complex geometry by breaking the entire geometry into simpler components and generating a nearly independent block of the grid for each component. For the wing/fuselage/nacelle/pylon configuration described in this paper, the primary components are the wing/fuselage, nacelle, pylon, and core-cowl. The grid generation for these primary components is accomplished using special-purpose methods which have undergone extensive development as part of this effort; these are described in the following paragraphs. The final complete grids also contain blocks representing such secondary components as core-cowl bifurcation, farfield block, etc. Since these were generated using more conventional methods, they will not be described in detail here.

Wing/Fuselage Grid

The grid in the wing/fuselage block is of modified C-O topology, in which J is in the streamwise direction, K is in the spanwise direction, and L is normal to the wing surface. It is generated by using conformal mapping and algebraic techniques[14] to construct the meshes on the first and last J, K, and L surfaces, as well as on several intermediate J surfaces. It then uses 3-D transfinite interpolation to fill in the grid points in the volumes bounded by these surfaces. The extensive use of conformal mapping on the surfaces (in particular on the fuselage, the symmetry plane, the farfield boundary, and the J surfaces) results in a grid of exceptional quality (orthogonality and smoothness). The transformation procedures and mapping functions are described in Ref. 15. The wing/fuselage grid in side and front views are

seen in Fig. 2a. A farfield grid is also generated to enlarge the computational domain, as seen in Fig. 2b.

Pylon Grid

The grid in the pylon block is of C-H topology, and because the pylon may wrap around the wing leading edge, special techniques must be employed. In the first step, a general-purpose surface-grid code is used to distribute grid points on the pylon surface. Due to the extreme skewness of this particular geometry an elliptic (Laplace) solver is needed. Next the geometry is transformed by unrolling the nacelle about its axis and unwrapping the wing about a singular point inside its leading edge to produce a distorted pylon extending between two quasiparallel walls (the images of the wing and the nacelle). Conformal mapping and algebraic techniques are used to generate C-type meshes on the wing and nacelle surfaces. The farfield boundary is then defined by connecting corresponding points on these two surfaces with straight lines. Transfinite interpolation then produces a 3-D grid in the transformed space, and the wing unwrapping and nacelle unrolling are performed in reverse to transform the grid back to physical space. The grid produced in this manner is shown in Fig. 2c.

Nacelle Grid

The grid in the nacelle block is also of C-O topology and is generated using another special-purpose code which cuts the nacelle with a series of planes extending from the nacelle centerline to the farfield boundary at various angles around the nacelle circumference. Next, conformal mapping techniques are used to generate a C-mesh in each plane. The primary transformation required unwraps the nacelle about a singular point just inside the leading edge, while simultaneously unwrapping the rectangular farfield boundary to a horizontal line. The grid produced in this manner can be seen in Fig. 2d.

Core-Cowl and Secondary Components Grids

Since the components of primary interest in this study involve the wing, nacelle (external), and pylon, the nacelle internal and core-cowl are modeled with Euler calculation meshes. The core-cowl grid is of C-O topology and is generated in a similar manner as the nacelle grid (except without the viscous layer). The core-cowl

bifurcation grid is broken into internal and external parts as seen in Fig. 2e. The internal part of the bifurcation extends from the nacelle internal top center to the top of the core-cowl. The external portion of the bifurcation comprises the lower portion of the pylon and intersects the internal part near the core-cowl trailing edge.

Grid Overlapping

To proceed with the analysis, the aforementioned individual grids are overlapped and a grid processing code PEGSUS[16], developed by CALSPAN of AEDC, is used to find the interpolation information between overlapping grids. In general, by defining proper hole creation boundaries, determining the interpolation information for the hole boundaries and the outer boundaries is straightforward. However, in very complex geometric regions where different grids have to be generated for individual components to simplify the grid generation effort, it may occur that two different components share a common solid surface. Here it is possible that incorrect hole boundaries may be determined due to inconsistency of the surface definition from the two different component grids. Particularly geometry juncture regions, such as the wing/pylon and pylon/nacelle junctions, are very susceptible to this problem, whic is an issue associated with Chimera grids.

Buning, et al., developed a unique grid procedure, called collar grids[17], to resolve this problem, whereby an extra O or C type grid is generated to wrap around the junction area, as seen in Fig. 3. Special programs have to be employed for generating this extra (collar) grid to ensure that one surface of the collar grid lies on the bi-linear body surface of the two adjacent components. In this manner, the grid points on the body surfaces (for the two adjacent components) can be cut cleanly and proper hole boundary interpolations can be obtained. One other advantage of using collar grids is that the viscous layer near the juncture region within the collar grid is represented in one grid direction, which simplifies the length scale estimation in the implementation of algebraic turbulence models.

In the current work, instead of using the regular collar grid approach, some of the individual grids, such as the pylon and the core-cowl bifurcation grids, were generated in a way that allows them to be used as the collar grids. For instance, at the wing/pylon and nacelle/pylon junctions, two

surfaces of the pylon grids lie on the bi-linear body surfaces of the wing and nacelle, respectively. By defining a hole-creation boundary within the pylon grid, the points on the wing and nacelle body surfaces which are located within this hole-creation boundary can then be cut cleanly. The hole boundaries for the wing and nacelle are shown in Fig. 4a. The hole boundaries for the nacelle and the core-cowl grids in the vertical symmetry plane are shown in Fig. 4b.

III. Numerical Procedures

Governing Equations

For high Reynolds number flow, the thin-layer approximation can be made and the conservation equations of mass, momentum, and energy can be represented as[18,19]:

$$\partial_\tau \hat{Q} + \partial_\xi \hat{E} + \partial_\eta \hat{F} + \partial_\zeta \hat{G} = Re^{-1}\left(\partial_\eta \hat{S}_1 + \partial_\zeta \hat{S}_2\right)$$

$$\hat{Q} = \frac{1}{J}\begin{bmatrix} \rho \\ \rho u \\ \rho v \\ \rho w \\ e \end{bmatrix} \qquad \hat{E} = \frac{1}{J}\begin{bmatrix} \rho U \\ \rho uU + \xi_x p \\ \rho vU + \xi_y p \\ \rho wU + \xi_z p \\ (e+p)U - \xi_t p \end{bmatrix}$$

$$\hat{F} = \frac{1}{J}\begin{bmatrix} \rho V \\ \rho uV + \eta_x p \\ \rho vV + \eta_y p \\ \rho wV + \eta_z p \\ (e+p)V - \eta_t p \end{bmatrix} \qquad \hat{G} = \frac{1}{J}\begin{bmatrix} \rho W \\ \rho uW + \zeta_x p \\ \rho vW + \zeta_y p \\ \rho wW + \zeta_z p \\ (e+p)W - \zeta_t p \end{bmatrix}$$

where τ is time and ξ, η, ζ are the generalized coordinates with z normal to the body surface. S_1 and S_2 are the viscous flux in η and ζ directions.

The ideal gas assumption is made as the pressure, density, and velocity components are related to the specific total energy, e, as follows:

$$p = (\gamma - 1)\left[e - \frac{1}{2}\rho\left(u^2 + v^2 + w^2\right)\right]$$

A few of the numerical issues regarding the Chimera approach are briefly addressed here. The non-conservative interpolation formulations for passing information between different grid zones remain a major drawback in terms of accuracy for the overset grid approach.

However, the use of proper domain decomposition strategies should minimize the induced errors introduced in the overlapping regions by avoiding interpolating in areas of large gradients and ensuring compatible grid cell sizes.

Another major obstacle encountered for the overset grid approach is the accurate surface integration of forces and moments. An improved surface integration procedure is currently under development at NASA Ames Research Center, which accounts more thoroughly for the holes and overlapped regions on the surface.

IV. Results and Discussions

The configuration chosen for study with OVERFLOW is an advanced low-wing subsonic transport aircraft with wing-mounted nacelle/pylon, for which extensive NTF wind-tunnel test data is available. Initially OVERFLOW was applied to the clean wing/fuselage with single grid zone for establishing useful guidelines which were applicable to the subsequent full-configuration (wing/fuselage/nacelle/pylon) analyses. These guidelines address computational aspects such as turbulence models, differencing algorithms, and code convergence characteristics, and are discussed in this section. All analysis results presented here were performed near cruise Mach number and lift conditions, but at lower than flight (wind-tunnel test) Reynolds number.

Turbulence Model

Currently, within the OVERFLOW code two turbulence models are implemented and have been tested extensively. The first, and probably the most well known, is the Baldwin-Lomax (BL) algebraic model[20]. The second model is the Baldwin-Barth (BB) one equation model[21]. Wing surface pressures obtained by using both models are compared with the NTF test data at two different angles-of-attack in Fig. 5. A mid-span double shock flow structure is observed in both the NTF data and the OVERFLOW predictions at the lower angle of attack. At the higher angle of attack it can be seen that the shock structure becomes single shock dominated. In general, both models are seen to perform well in terms of predicting the pressure distributions and shock locations for the two inboard stations. For the two stations further outboard, the predicted shock locations are too far downstream, but the BB model is seen to perform slightly better than the BL model. This

observation, coupled with the fact that the BB model has no length scale requirement (which is a major advantage, especially for complex geometry juncture region calculations), led to the selection of the BB turbulence model for use in the analyses presented in the remainder of this paper.

Differencing Scheme

In general, compared to central differencing schemes, upwind schemes have the advantages of sharpening shock waves by capturing gradients in fewer grid points, and requiring no artificial dissipation.

Currently, central differencing and Roe's upwind schemes are available within the OVERFLOW code[22]. OVERFLOW computational studies with both schemes were conducted, and the predicted wing pressure distributions are compared with NTF test data at low and high angles-of-attack in Fig. 6. The central differencing scheme is seen to correlate better with the NTF data, especially over the aft portions of the airfoil and for the outboard wing stations (where the upwind scheme is seen to over-predict the shock strength and location). This result is unexpected, and may be related to trailing edge grid spacing. While further investigation is needed, a more accurate solution is obtained on this grid using central differencing. Furthermore, these analyses revealed that the central differencing scheme requires about 15-20% less CPU time compared to the upwind scheme. Therefore, the remainder of the OVERFLOW results presented in this paper were obtained with the more advantageous central differencing scheme.

Code Convergence

In OVERFLOW, a local time step scaling based on the metric Jacobian is employed to improve the convergence rate. The time step h is defined as:

$$h = DT \frac{0.005 + \sqrt{V}}{1 + \sqrt{V}}, \quad \text{where} \quad V = \frac{1}{J}$$

V is the cell volume and J is the Jacobian. The 0.005 factor is used to keep the time step from going to roundoff for very tiny cells.

CFL number minimum and maximum limits are also added into the code to further accelerate the convergence rate. For example, at the outer flowfield, the large grid cell size results in a very small CFL number. Carefully setting the CFL number can increase the time step and speed up the convergence rate for the inviscid portion of the flowfield. This often helps the boundary layer flow to converge. Our practical experience has shown this option to be very helpful in accelerating the overall convergence rate.

A typical OVERFLOW convergence history can be seen in Fig. 7, where the wing/fuselage grid residual (defined as the l_2-norms of the right hand side) and the wing surface lift coefficient are plotted against iteration number. The residual is seen to drop about 3 orders of magnitude, and the lift converges in less than 2000 iterations.

Installed Results

Having established OVERFLOW guidelines from the wing/fuselage analyses, the installed wing/fuselage/nacelle/pylon configuration analyses were conducted using the central differencing scheme with Baldwin-Barth turbulence model at representative Mach 0.85 cruise conditions. The OVERFLOW predicted installed (w/f/n/p) and clean (w/f) wing surface pressures are compared with corresponding NTF test data in Fig. 8, revealing significant engine installation effects, as well as excellent agreement of the predictions with the NTF data. The installation of the nacelle/pylon is seen to result in the formation of a mid-chord shock wave on the inboard portion of wing, while inducing increased aft acceleration and shock formation over the outboard portions. Furthermore, both the predicted and measured pressure distributions show a nacelle/pylon induced acceleration in the inboard leading edge region, and a deceleration in the outboard leading edge region. The significant wing upper surface flow field modification induced by the nacelle/pylon installation is further clarified by the OVERFLOW predicted pressure contours seen in Fig. 9. The nacelle/pylon addition is seen to disrupt the largely shock-free clean wing contours through the formation of an unswept inboard shock and an outboard double shock. These nacelle/pylon induced shock formations result in degraded wing performance and underscore the necessity of including the nacelle/pylon influence in any advanced wing design processes.

The numerical calculations in the current work were conducted on the NASA NAS Cray C-90 supercomputer with SSD. The complete installed wing/fuselage/nacelle/pylon mesh

consists seven grid zones and a total of ~1.7 million grid points. The OVERFLOW analysis required about 12 CPU seconds for one iteration and approximately 1500 iterations to converge.

V. Conclusions

The OVERFLOW/PEGASUS CFD methods have been successfully applied to complex full configuration wing/fuselage/nacelle/pylon geometries, demonstrating the capability of this procedure to provide thin-layer Navier-Stokes solutions about complex geometric configurations. The correlations with test data obtained for the computationally less intensive clean wing/fuselage case indicate that the best results for the advanced wings are currently achieved with the Baldwin-Barth turbulence model, used in conjunction with the central differencing option of the code. Subsequent OVERFLOW results obtained for the full configuration wing/fuselage/nacelle/pylon geometry correlate very well with corresponding test data, illustrating the unique capability of this code to accurately predict propulsion-airframe integration effects. The magnitude of the propulsion-installation induced wing-flow-field modifications underscores the pertinence of complete configuration analysis and wing design strategies.

Acknowledgements

References

1. Frink, N.T., Parikh, P., and Pirzadeh, S., "Aerodynamic Analysis of Complex Configurations Using Unstructured Grids," AIAA Paper 91-3292, September 1991.

2. Jameson, A. and Baker, T.J., "Improvements of the Aircraft Euler Method," AIAA Paper 87-0452, January 1987.

3. Thompson, J.F., Warsi, Z.U.A., and Mastin, C.W., "Numerical Grid Generation, Foundations and Applications," North-Holland, New York, pp. 306-309, 1985.

4. Sorenson, R.L., "The 3DGRAPE Book: Theory, User's Manual, Examples," NASA TM 102224, July 1989.

5. Chan, W.M., Chiu, I.T., and Buning, P.G., "User's Manual for the HYPGEN Hyperbolic Grid Generator and the HGUI Graphical User Interface," NASA TM 108791, October 1993.

6. Vatsa, V.N., Sanetrik, M.D., and Parlette, E.B., "Development of a Flexible and Efficient Multigrid-Based Multiblock Flow Solver," AIAA Paper 93-0677, January 1993.

7. Rai, M.M., "A Conservative Treatment of Zonal Boundaries for Euler Equation Calculations," J. of Comput. Phys., 62, pp. 472-503, 1986.

8. Benek, J.A., Steger, J.L., and Dougherty, F.C., "A Flexible Grid Embedding Technique with Application to the Euler Equations," AIAA Paper 83-1944, July 1983.

9. Buning, P.G., Chiu, I.T., Obayashi, S., Rizk, Y.M., and Steger, J.L., "Numerical Simulation of the Integrated Space Shuttle Vehicle in Ascent," AIAA Paper 88-4359-CP, August 1988.

10. Rogers, S.E., "Progress In High-Lift Aerodynamic Calculations," AIAA Paper 93-0194, January 1993.

11. Buning, P.G., Chan, W.M., Renze, K.J., Sondak, D., Chiu, I.T., and Slotnick, J.P., "OVERFLOW User's Manual, Version 1.6xx" NASA Ames Research Center, Moffett Field, CA, 1991.

12. Benek, J.A., Buning, P.G., and Steger, J.L., "A 3-D Chimera Grid Embedding Technique," AIAA Paper 85-1523, July 1985.

13. Steger, J.L. and Benek, J.A., "On the Use of Composite Grid Schemes in Computational Aerodynamics," NASA TM 88372, November 1986.

14. Halsey, N.D., "Use of Conformal Mapping in Grid Generation for Complex Three-Dimensional Configurations," AIAA J., Vol. 25, No. 10, p. 1286 October 1987.

15. Halsey, N.D., "Strategies for Applying 2-D Conformal Mappings to 3-D Grid Generation Problems," to be presented at 14th IMACS World Congress on

Computation and Applied Mathematics, July 1994.

16. Suhs, N. E., and Tramel, R. W., "PEGSUS 4.0 User's Manual," AEDC-TR-91-8, Arnold AFB, TN, November 1991.

17. Parks, S. J., Buning, P. G., Steger, J. L., and Chan, W. M., "Collar Grids For Intersecting Geometric Components Within the Chimera Overlapped Grid Scheme," AIAA-91-1587-CP, pp.672-682, June 1991.

18. Viviand, H., "Forms Conservatives des Equations de la Dynamique des Gaz," La Recherche Aerospatiale, No. 1, pp.65-68, Jan.-Feb. 1974.

19. Pulliam, T. H. and Steger, J. L., "Implicit Finite-Difference Simulations of Three-Dimensional Compressible Flow," AIAA J., Vol. 18, No. 2,pp.159-167, 1980.

20. Baldwin, B. S. and Lomax, H., "Thin Layer Approximation and Algebraic Model for Separated Turbulent Flows," AIAA Paper 78-257, January 1978.

21. Baldwin, B. S. and Barth, T., "A One-Equation Turbulence Transport Model For High Reynolds Number Wall-Boundary Flows," NASA TM 102847, August 1990.

22. Kandula, M. and Buning, P. G., "Implementation of LU-SGS Algorithm and Roe Upwinding Scheme in OVERFLOW Thin-Layer Navier-Stokes Code," AIAA-94-2357, AIAA 25th Fluid Dynamics Conference, June 1994.

Aft View

Front View

nacelle

pylon

wing

core-cowl
bifurcation

core-cowl
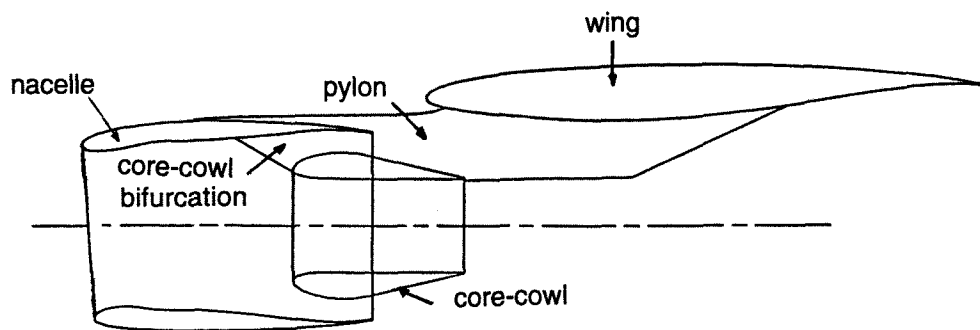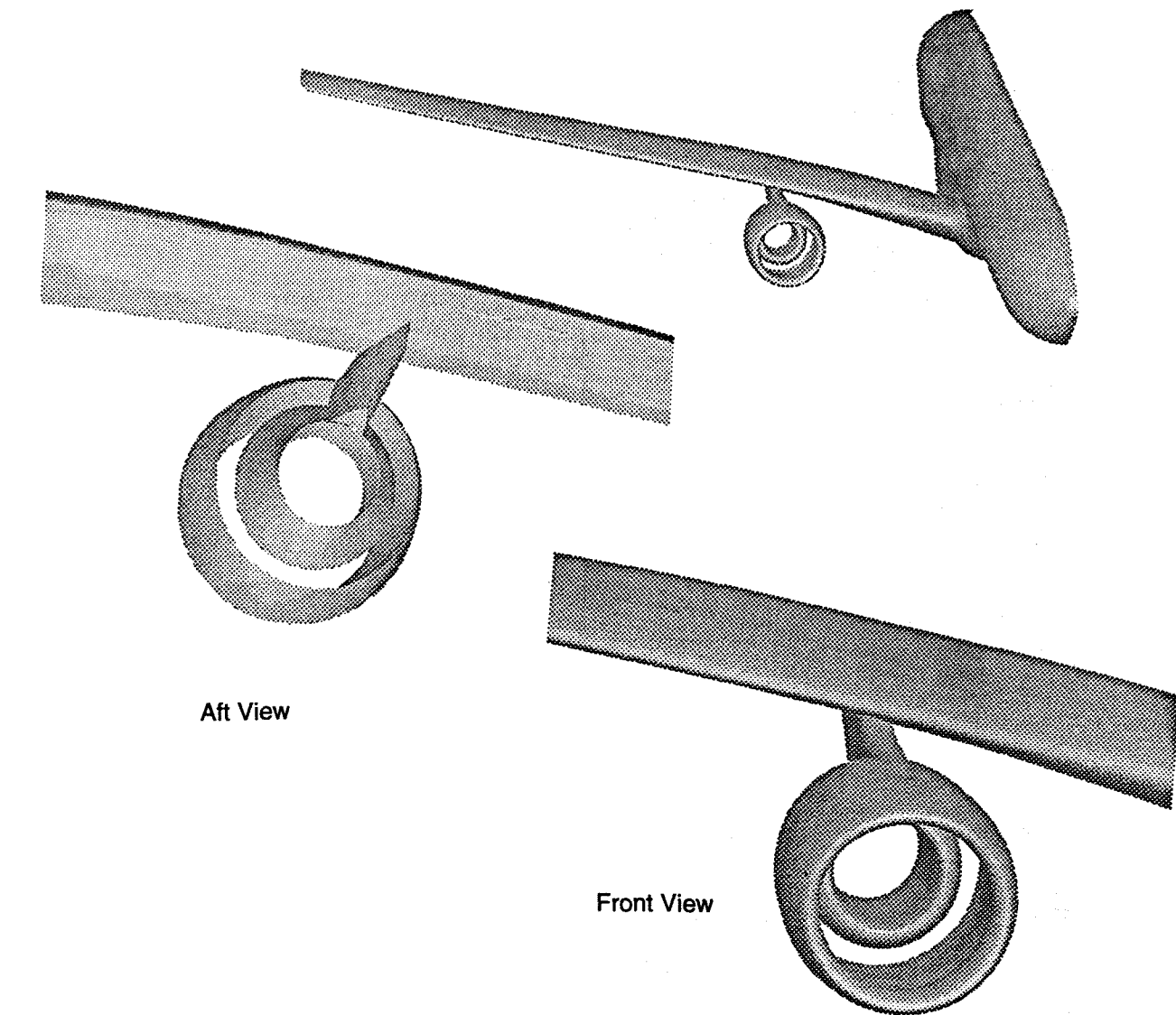
Figure 1. Wing/Fuselage/Nacelle/Pylon configuration
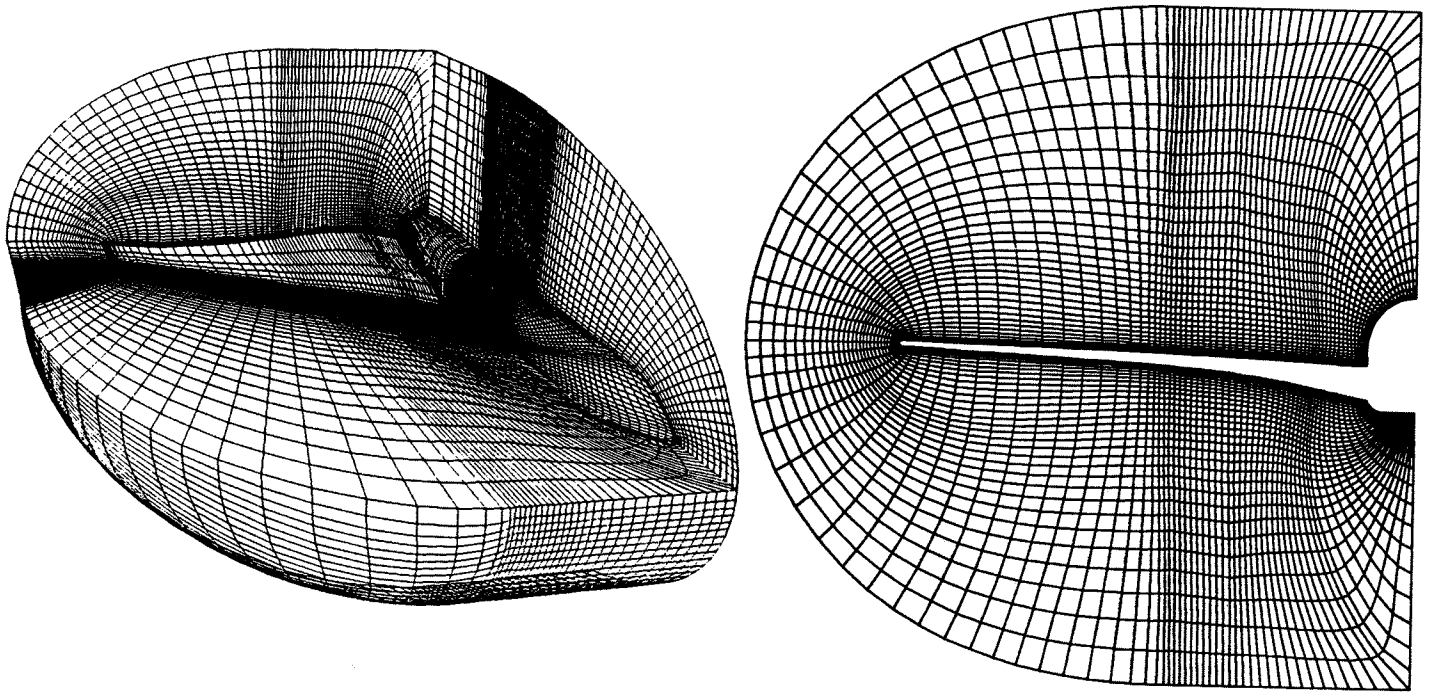
Figure 2a. Wing/Fuselage grid in isometric and front views
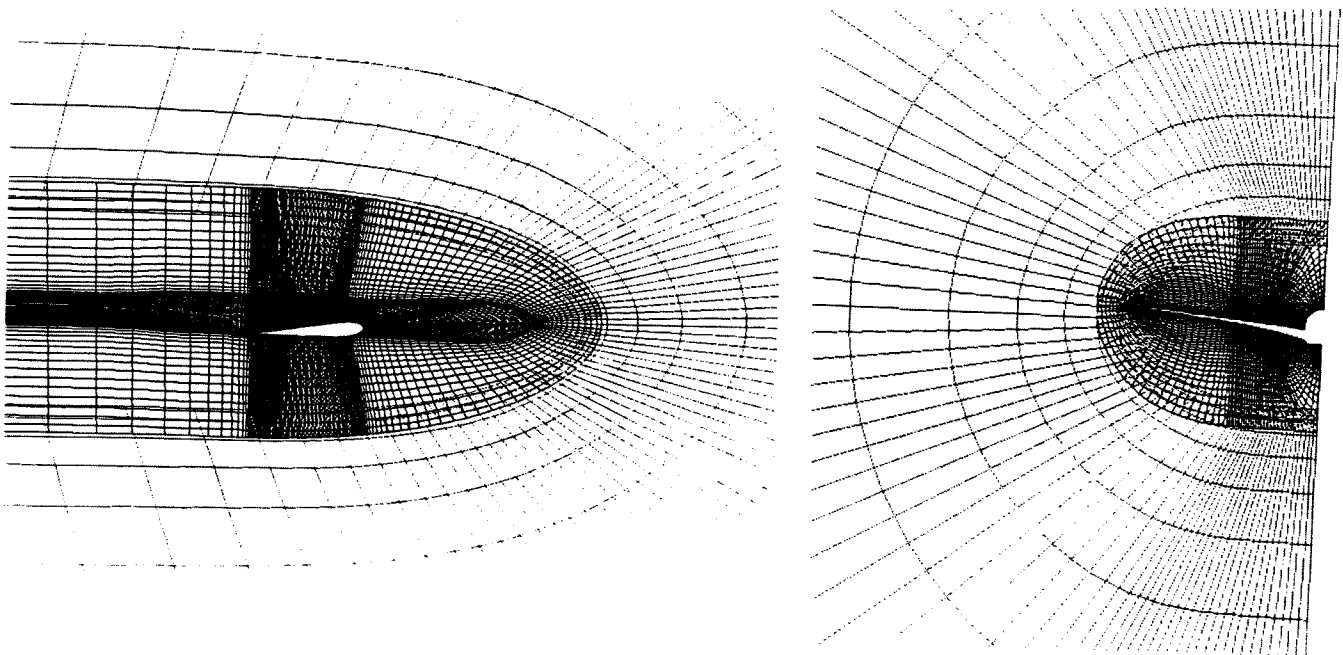
Figure 2b. Farfield and wing/fuselage grid overlap region in side and front views

2428

Wing Surface
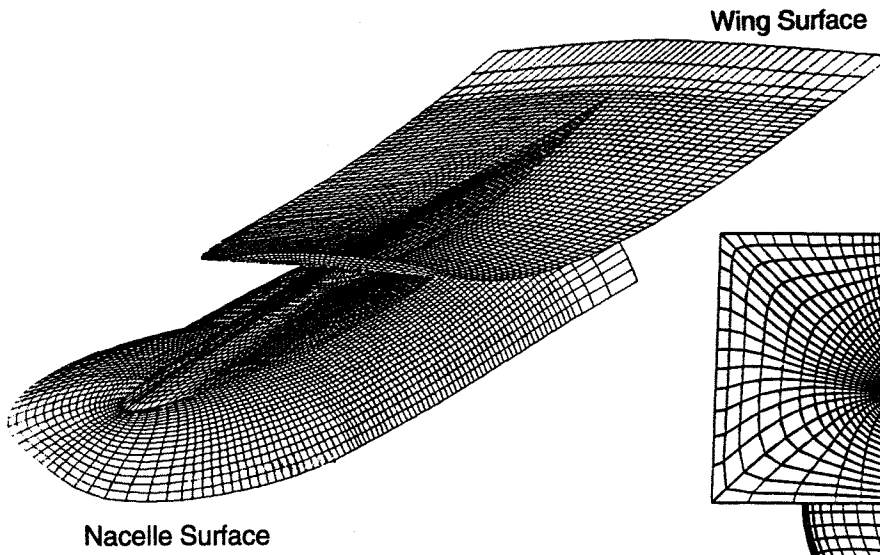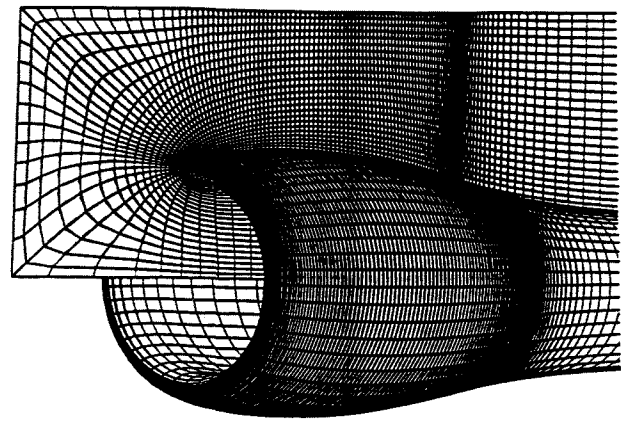
Nacelle Surface

Figure 2c. Pylon grid

Figure 2d. Nacelle grid

External

Internal

External

Internal

Front Isometric

Aft Isometric
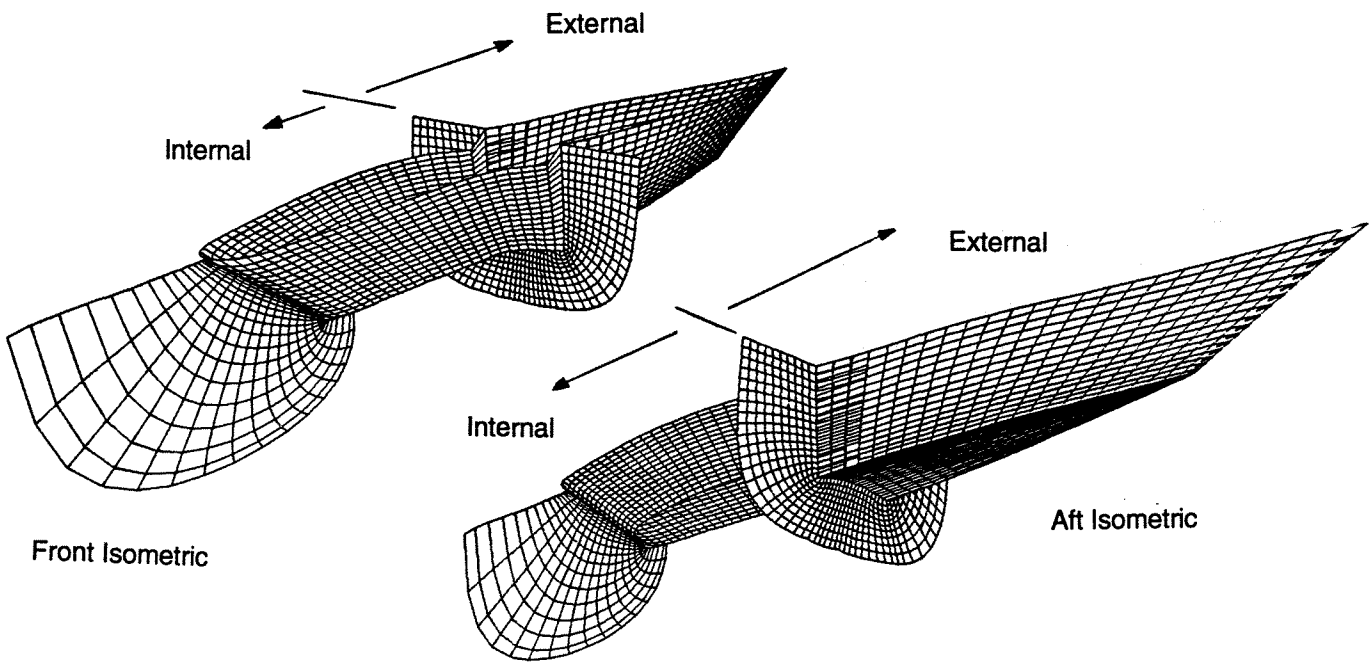
Figure 2e. Core-cowl bifurcation grid

body 1

body 2

surface grid on two adjoining bodies

complete collar grid
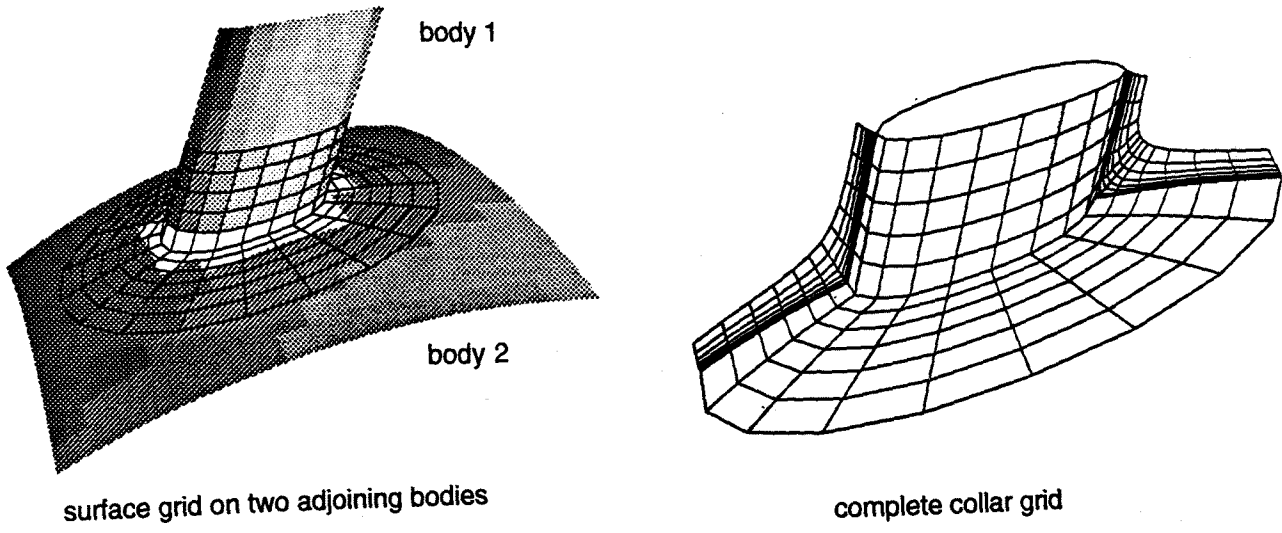
Figure 3. Sample collar grid
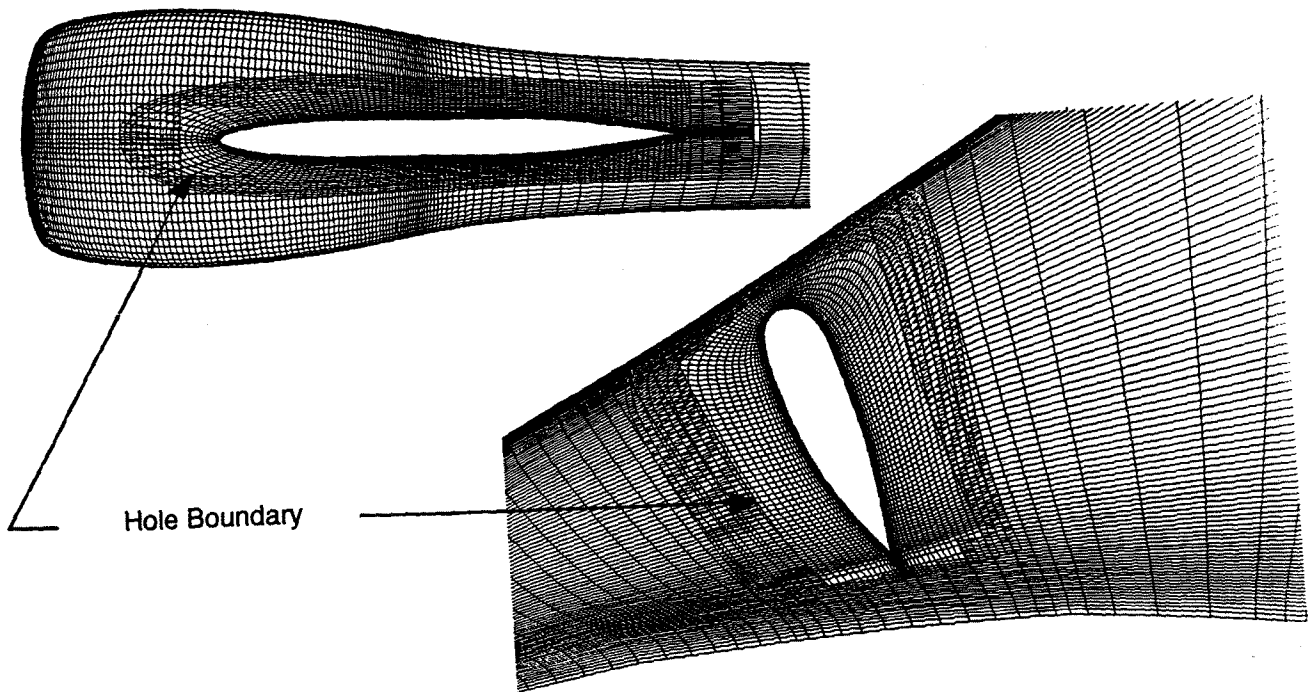
Hole Boundary

Figure 4a. Hole boundaries on wing/pylon and nacelle/pylon intersection surfaces

2430
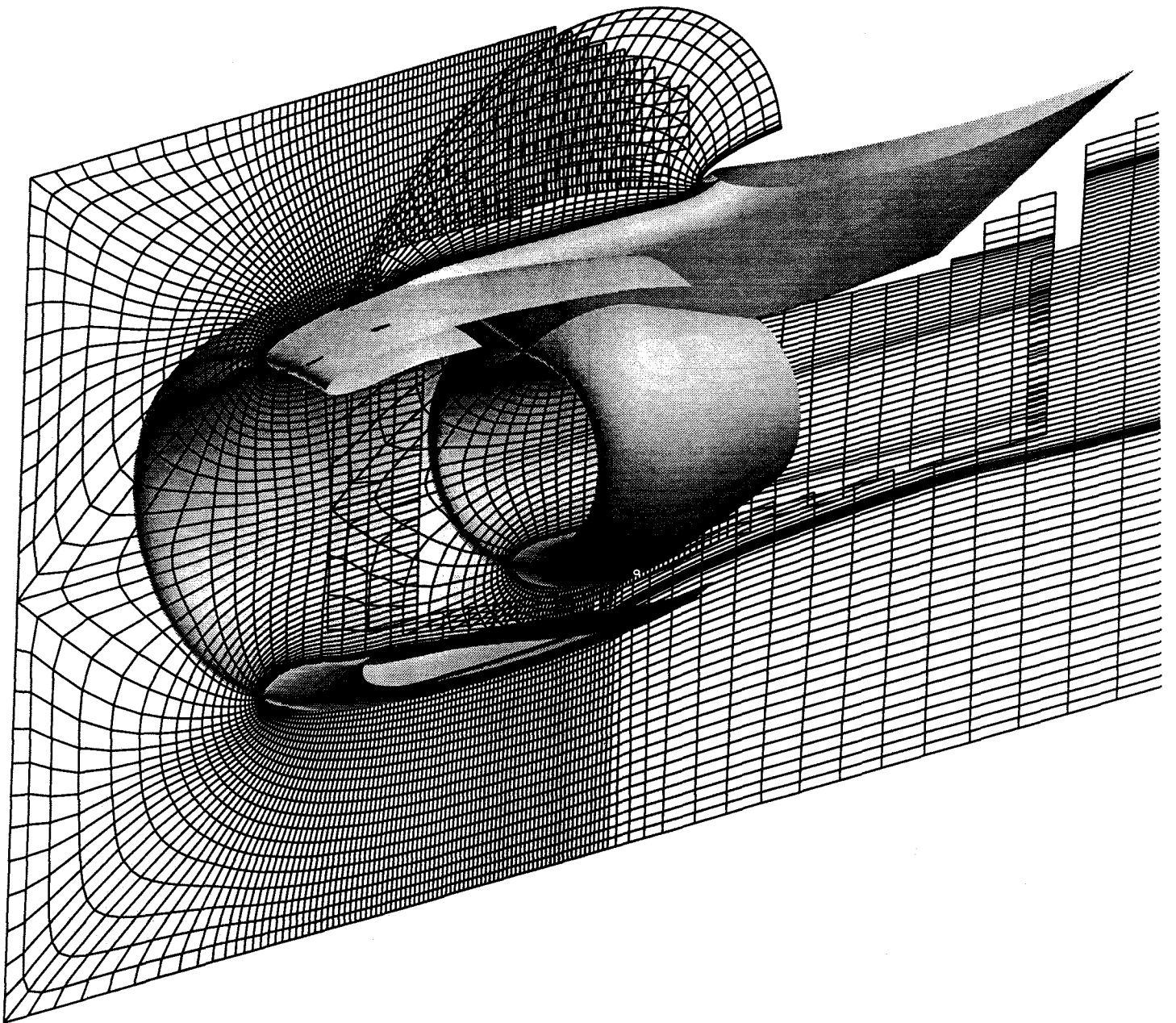
Figure 4b. Hole boundaries for nacelle and core-cowl grids in the vertical symmetry plane
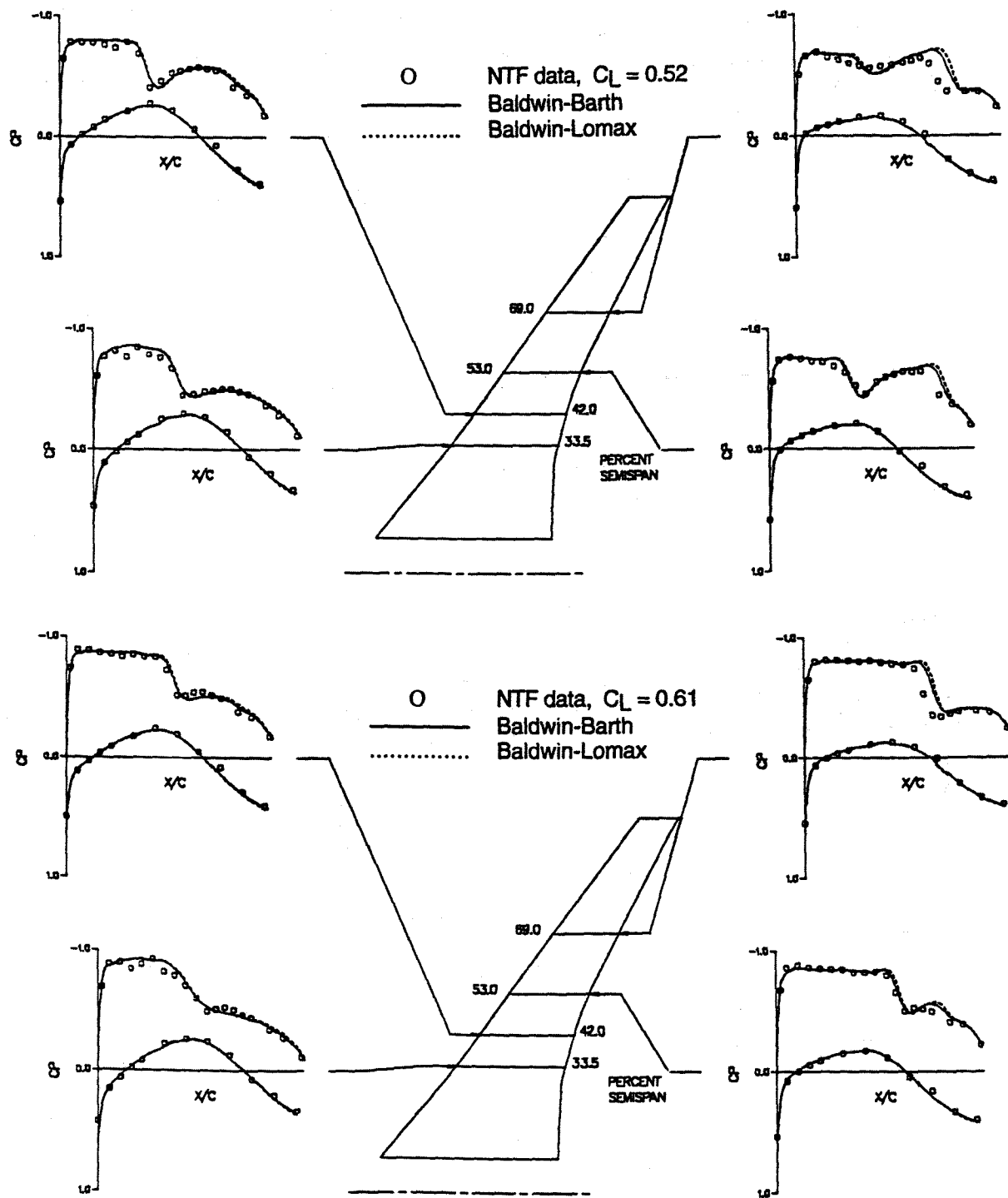
Figure 5. Baldwin-Lomax vs. Baldwin-Barth wing pressure distributions
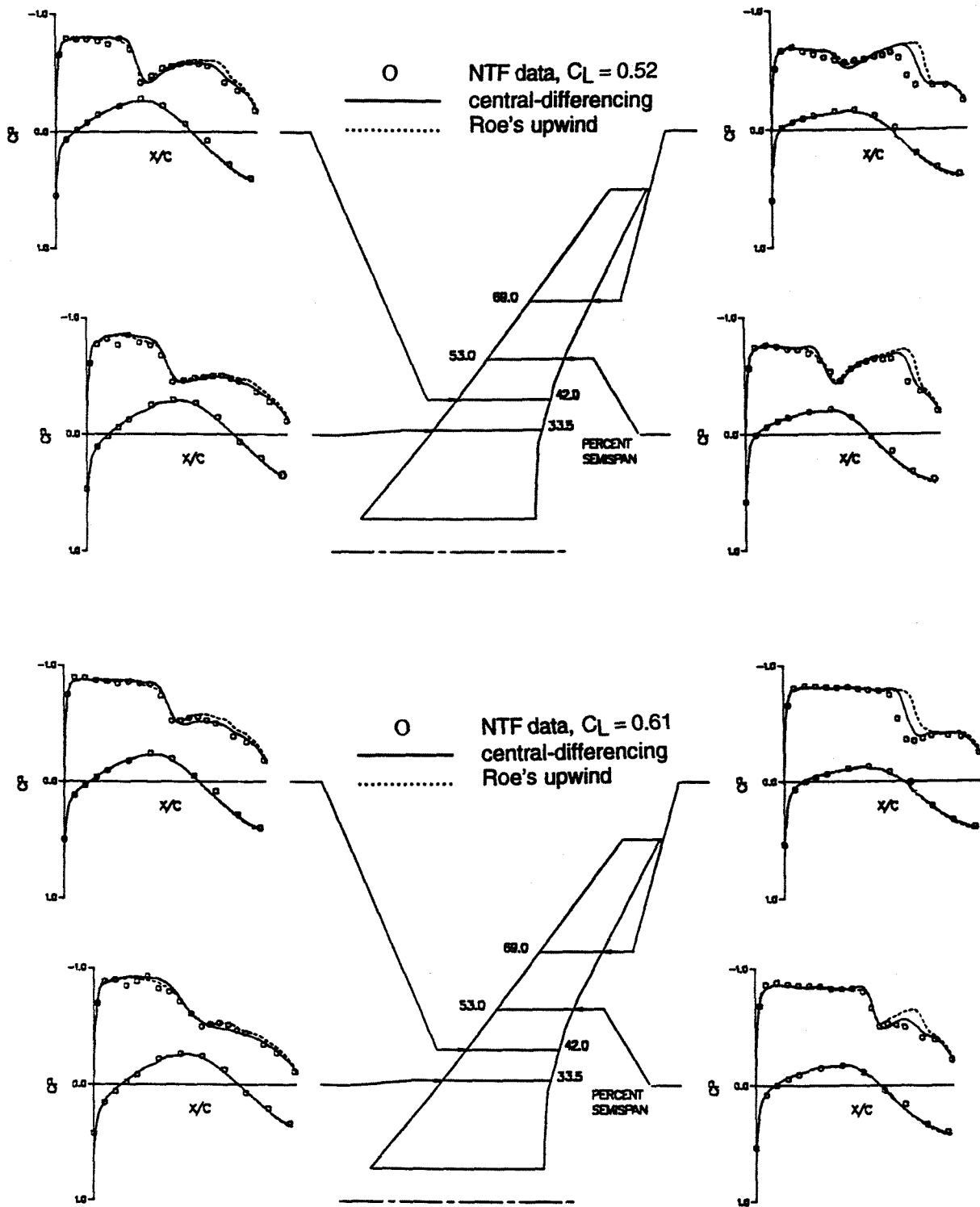for advanced wing/fuselage configuration
$M_\infty = 0.85$, Re = 4.3 million

Figure 6. Central vs. Roe's upwind wing pressure distributions
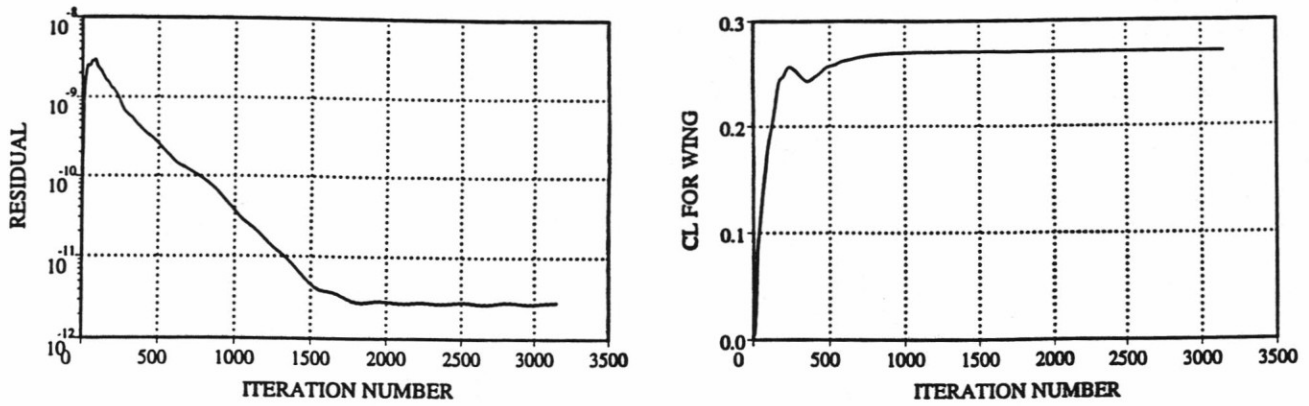for advanced wing/fuselage configuration
$M_\infty = 0.85$, Re = 4.3 million

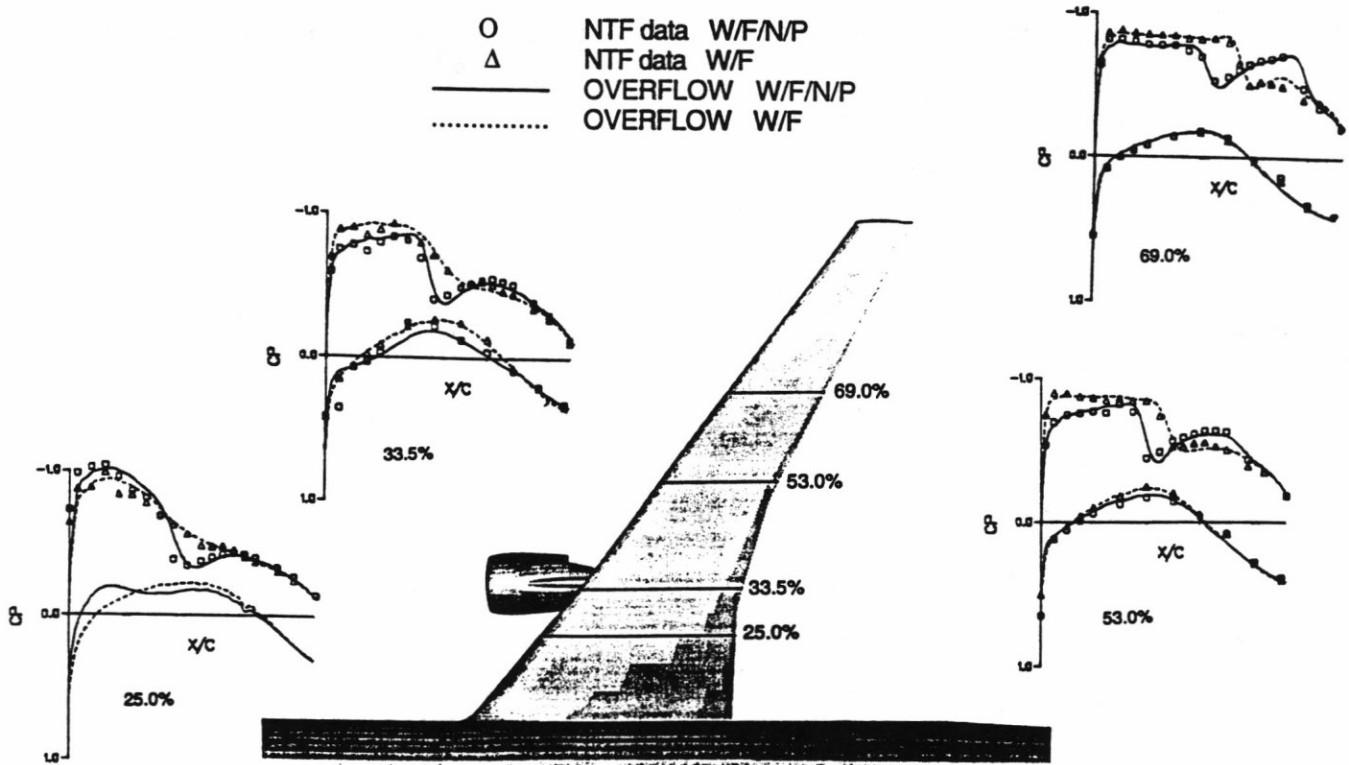Figure 7. Convergence history for wing/fuselage grid

Figure 8. Clean (W/F) vs. Installed (W/F/N/P) wing pressure distribution comparisons to test data
Central-differencing scheme with Baldwin-Barth turbulence model
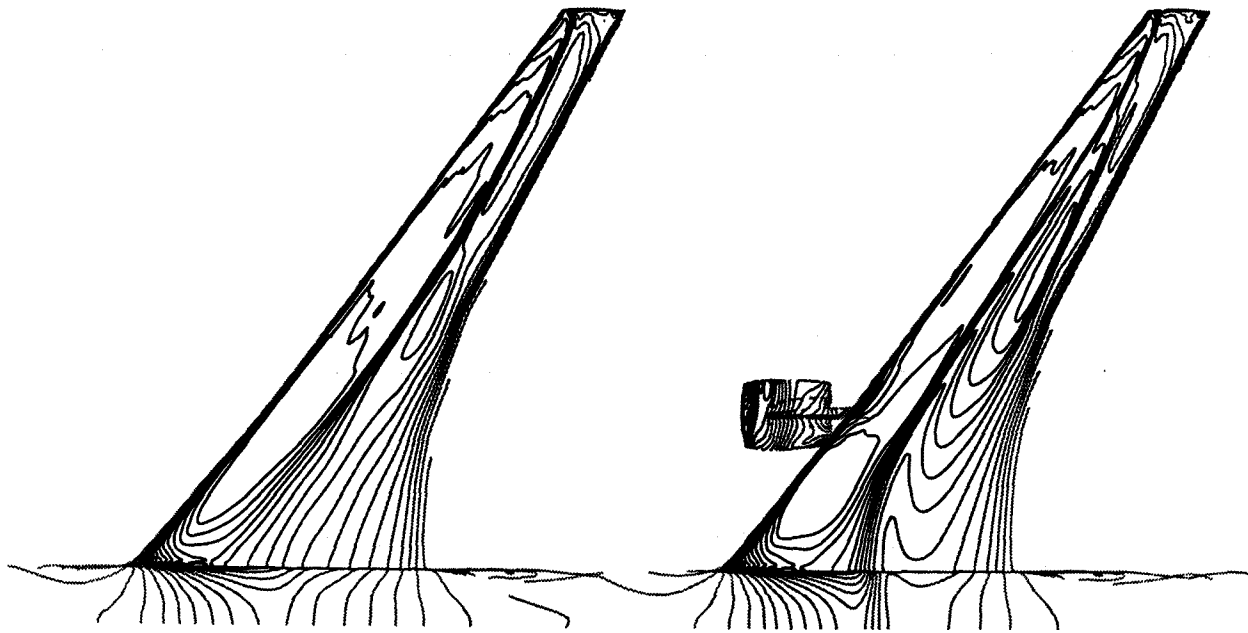$M_\infty = 0.85$, $C_L = .61$, Re = 4.3 million

Figure 9. Clean (W/F) vs. Installed (W/F/N/P) wing upper surface pressure contours
$M_\infty = 0.85$, $C_L = .61$, Re = 4.3 million